ORIGINAL ARTICLE

Addiction Biology   SSA   WILEY

Functional connectivity in reward-related networks is associated with individual differences in gambling strategies in male Lister hooded rats

Nikita Tjernström[1] 🄳 | Tie-Qiang Li[2,3] | Sarah Holst[4] | Erika Roman[1,5] 🄳

[1]Research Group Neuropharmacology, Addiction and Behavior, Department of Pharmaceutical Biosciences, Uppsala University, Uppsala, Sweden

[2]Department of Clinical Science, Intervention and Technology, Karolinska Institutet, Stockholm, Sweden

[3]Department of Medical Radiation and Nuclear Medicine, Karolinska University Hospital, Solna, Sweden

[4]Department of Neuroscience, Karolinska Institutet, Stockholm, Sweden

[5]Department of Anatomy, Physiology and Biochemistry, Swedish University of Agricultural Sciences, Uppsala, Sweden

Correspondence
Nikita Tjernström, Department of Pharmaceutical Biosciences, Uppsala University, Box 591, 751 24 Uppsala, Sweden.
Email: nikita.tjernstrom@farmbio.uu.se

Abstract

Individuals with gambling disorder display deficits in decision-making in the Iowa Gambling Task. The rat Gambling Task (rGT) is a rodent analogue that can be used to investigate the neurobiological mechanisms underlying gambling behaviour. The aim of this explorative study was to examine individual strategies in the rGT and investigate possible behavioural and neural correlates associated with gambling strategies. Thirty-two adult male Lister hooded rats underwent behavioural testing in the multivariate concentric square field™ (MCSF) and the novel cage tests, were trained on and performed the rGT and subsequently underwent resting-state functional magnetic resonance imaging (R-fMRI). In the rGT, stable gambling strategies were found with subgroups of rats that preferred the suboptimal safest choice as well as the disadvantageous choice, that is, the riskiest gambling strategy. R-fMRI results revealed associations between gambling strategies and brain regions central for reward networks. Moreover, rats with risky gambling strategies differed from those with strategic and intermediate strategies in brain functional connectivity. No differences in behavioural profiles, as assessed with the MCSF and novel cage tests, were observed between the gambling strategy groups. In conclusion, stable individual differences in gambling strategies were found. Intrinsic functional connectivity using R-fMRI provides novel evidence to support the notion that individual differences in gambling strategies are associated with functional connectivity in brain regions important for reward networks.

KEYWORDS
behaviour, functional connectivity metrics, multivariate concentric square field, novel cage, rat gambling task, resting-state fMRI

1 | INTRODUCTION

Gambling problems are important health concerns. The prevalence of problematic gambling, including both problem gambling and gambling disorder (GD), is around 0.1%–5.8% worldwide.[1] Whereas problem gambling usually is based on self-reports of past behaviour, GD is a diagnosis in the category Substance-Related and Addictive Disorders in the Diagnostic and Statistical Manual of Mental Disorders, 5th Edition (DSM-5). Thus, GD is the first non-substance addictive disorder to be included in the addiction category.[2] Problem gambling and GD share features with alcohol and substance use disorders, such as clinical manifestation, underlying personality traits and pharmacological treatment options.[3–6] Moreover, similarities in neurobiological characteristics have been found, for example, altered processing in the brain reward networks.[7]

In humans, the Iowa Gambling Task (IGT) is used to study impaired decision-making.[8] Poor performance on the IGT is predictive of problem gambling,[9] and individuals with GD display deficits in decision-making when performing the IGT.[10,11] Rodent tests have provided important contributions in studies of decision-making processes.[12] The rat Gambling Task (rGT) is the rodent analogue to the IGT, and the outline of the test corresponds to the IGT, with four choices associated with wins or losses. Four different versions of the rGT have been developed with slightly different focus, advantages and disadvantages.[13] The rGT used in this study involves sucrose pellets as reward and time-out periods as punishment.[14,15] From a translational value, it is important to note that rats appear to use strategies in the rGT that resembles those used by humans in the IGT.[12] However, in studies conducted so far in rats, the main focus has been on factors and treatments that attenuate the disadvantageous options in favour of the more advantageous choices.[15–18] Studies on individual differences in gambling strategies, underlying behavioural endophenotypes and neural correlates are prerequisites for an understanding of features in problem gambling and GD. This novel approach is of focus herein.

Human data reveal that patients with GD express a more risk-taking behaviour,[19,20] although diverging results regarding the relationship between decision-making in the rGT and risk-taking behaviour have been found in rats.[21–24] This discrepancy may be due to the limitation of many conventional tests in capturing risk-taking behaviour. Moreover, in rats, little is known about behavioural traits associated with individual differences in gambling strategies. Therefore, two ethologically founded exploration based tests were used herein, that is, the multivariate concentric square field™ (MCSF)[25,26] and novel cage[27] tests. The MCSF arena contains areas of different environmental qualities that give the animal opportunity to display behaviours associated with general activity, exploration, risk assessment, risk-taking and shelter-seeking and thereby generate a behavioural profile.[25,26] The MCSF test has previously been useful in studies of subgroups of rats with different behavioural profiles associated with high and low propensity for voluntary alcohol intake[28] and different potassium- and amphetamine-induced dopamine responsivity.[29]

Decision-making depends on a complex interplay between several neural systems. A study on healthy volunteers performing the IGT during functional magnetic resonance imaging (fMRI) scanning revealed activity in several areas associated with brain reward networks, including the prefrontal cortex, cingulate cortex and nucleus accumbens.[30] Moreover, Clark et al reviewed the neuroimaging literature and concluded that dysregulation in several brain regions has been linked to GD. Furthermore, the neuroimaging profiles of patients suffering from GD and substance use disorders shared similar vulnerability markers.[31] Functional connectivity networks in the human brain assessed using resting-state fMRI (R-fMRI) are consistent with fMRI results invoked by external stimuli. A recent study by Gratton et al investigated variations in the brain functional networks and found that these networks possessed day-to-day stability for individual subjects. Most of the variations were due to individual differences, although the tasks and sessions had little impact on the fMRI results.[32]

Studies in rodents have demonstrated corresponding neuronal networks.[33,34] However, little is known about the behavioural and neural mechanisms that drive some individuals to make risky or advantageous decisions. To the best of our knowledge, this is the first study utilizing R-fMRI to study brain functional connectivity networks in rats following behavioural testing and evaluation of gambling strategies in the rGT. It was of particular interest to explore how brain functional networks vary in individuals with different gambling strategies. Therefore, the aim of this study was to explore individual differences in the rGT and investigate possible behavioural predictors and neural correlates of the different strategies in the rGT.

2 | MATERIAL AND METHODS

2.1 | Animals and housing

Male Lister hooded rats (HsdOla:LH, Envigo, Horst, the Netherlands, $n = 32$) were delivered at 5–6 weeks of age. The animals were pair-housed in transparent cages Type IV (59 × 38 × 20 cm) with raised lids containing wood chip bedding. For enrichment purposes, each cage had paper sheets (40 × 60 cm, Cellstoff, Papyrus) and a wood tunnel. The cages were kept in an animal room on reversed light/dark cycle (lights off at 6:00 am) with a masking background noise. The animal room was kept in constant temperature (22 ± 1°C) and humidity (50 ± 10%). The animals had access to rat chow (Type R36, Lantmännen, Kimstad, Sweden) ad libitum before and after the rGT. During all parts of the rGT, the rats were food restricted to 85% of their free feeding weight and maintained on 14 g of rat chow given 1 h after their gambling session. The chow was spread out in the cage to secure access for both individuals in a pair. Body weight of the animals (Figure 1A) was closely monitored to ensure that the food restriction was properly carried out. Water was available ad libitum during the whole experiment.

All animal experiments were approved by the Uppsala Animal Ethical Committee (permit number 5.8.18-00833/2017) and followed the guidelines of the Swedish Legislation on Animal Experimentation (Animal Welfare Act SFS 1998:56) and the European Union Directive on the Protection of Animals Used for Scientific Purposes (Directive 2010/63/EU).
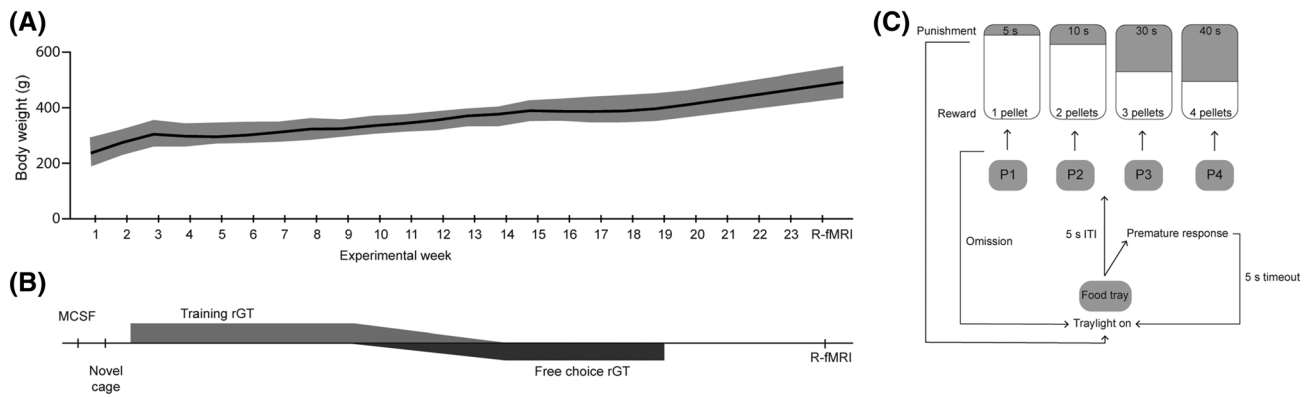
FIGURE 1 (A,B) Rat population ($n = 32$) body weight (g; A) and the outline of the experiment (B) over the corresponding experimental weeks. (A) The population mean body weight is displayed by the black line, and the grey shadow shows the body weight range. (B) The order of the different tests is shown corresponding to the weeks on the x-axis of Figure 1A. The time required to complete training prior to the free choice rGT differed between animals and is indicated by the overlap between training and free choice rGT, that is, the first individual finished training and moved on to free choice rGT during Week 9 and the last animal during Week 14. (C) Schematic of the rat gambling task (rGT). The size of the white and grey parts of the reward/punishment blocks indicates the probability of reward and punishment for each choice (P1–P4). The contingencies with regard to reward probability, number of pellets and duration of punishing time-outs for the different options were: P1 $p = 0.9$, 1 and 5 s; P2 $p = 0.8$, 2 and 10 s; P3 $p = 0.5$, 3 and 30 s; P4 $p = 0.4$, 4 and 40 s. ITI, inter-trial interval; MCSF, multivariate concentric square field™ test; rGT, rat gambling task; R-fMRI, resting-state functional magnetic resonance imaging

2.2 | Experimental outline

An experimental outline is shown in Figure 1B. After delivery, the animals were left undisturbed for 2 weeks to acclimate to the animal facility and the reversed light/dark cycle.[35] During the following week, the rats were handled on 3 consecutive days to habituate to the experimenter and the daily procedures. The handling consisted of individual handling, weighing and adaptation to the transportation bucket used to transport the animals to the behavioural testing room. During this week, the rats were individually marked by ear punching. The behavioural tests were carried out the following 2 weeks, first the MCSF and 1 week later the novel cage test. The animals were tested in the same order in both tests. One rat in each pair was tested first across all cages followed by the second rat across all cages. Before training for the rGT, the animals were habituated to the operant chambers. For the last part of the study, the animals were transported by truck to the MRI facility. After transport, they were again left undisturbed for 2 weeks to acclimate to the animal facility. Due to time constraints, 30 animals underwent the R-fMRI scan; the two animals that were excluded were the last ones to accomplish the rGT training. The body weight of the animals was continually monitored (Figure 1A): weekly during the behavioural testing, daily during rGT, and a measurement was taken before the MRI scan.

2.3 | MCSF test

The MCSF test has been described in detail elsewhere.[26] Briefly, the apparatus is 100×100 cm with walls that divide it into different parts (Figure S1). In the middle of the apparatus is an open area called centre (70×70 cm). During analysis, a central circle (CTRCI; 25 cm in diameter) is added in the centre for interpretation of risk-taking versus thigmotaxic behaviour. From the centre, three corridors are accessible, which in turn lead to different areas; a sheltered area called the dark corner room (DCR); an elevated area called the hurdle, which contains a hole board with two holes for the animal to nose poke into as an explorative incentive; and an elevated and brightly lit bridge construction with stainless-steel wire-mesh floor. The beginning of the bridge is called slope and is accessible from the corridor. The lighting conditions (lux) in the arena were as follows: centre and corridors <30, DCR <0.5 and bridge >500. When testing began, the animal was placed in the centre facing the wall without a corridor entry and was allowed to explore the arena during 20 min. In between animals, the arena was cleaned with 10% ethanol and left to dry.

2.4 | Novel cage test

The novel cage test[27] consisted of a cage ($38 \times 38 \times 31$ cm) that the individual has never experienced before. The floor of the cage is covered with wood chip bedding (7 cm deep). The rat was released in the middle of the cage and allowed to freely explore for 5 min. An ethogram of behaviours scored is shown in Table S1. The bedding was changed, and the walls were cleaned with 10% ethanol solution and left to dry in between animals.

2.5 | Behavioural recordings

The MCSF and novel cage test sessions were recorded by an overhead camera and the experimenter observed from an adjacent room. Descriptive parameters were generated using the EthoVision system

(Version XT 12.0, Noldus Information Technology, Wageningen, the Netherlands). For the MCSF test, the total distance (cm) moved and mean velocity (cm/s) in the arena were tracked automatically. Automatic tracking was also used to determine the latency to first visit(s), duration(s) and frequency of visits to the defined zones (except for slope and bridge that were scored manually due to poor detection). Frequency of rearing, grooming, nose pokes into the hole board holes and stretched attend postures (SAPs) were scored manually. The following parameters were derived: latency to leave centre (Lat leave), duration per frequency in all zones (D/F), sum of all frequencies (total activity; TOTACT), duration and frequency in the corridors (D and F TOTCORR, respectively) and percentage duration and frequency in all zones (%D and %F, respectively). The novel cage test duration(s) and frequency of behaviours described in Table S1 were scored manually.

2.6 | rGT

2.6.1 | Apparatus

The rGT took place in five-hole operant chambers (34 × 33 × 33 cm) placed inside ventilated sound-attenuating cabinets (56 × 56 × 70 cm; Med Associates, Inc.). The chambers included five response holes, a food tray and a house light. Only four response holes are used in the rGT; therefore, the middle response hole was not used during training or testing. A response in that hole was not recorded as a choice or a premature response. However, responses in that hole were included in the measurements preservative responses and total head entries during punishment, which are described in the rGT section. Both the response holes and the food tray were equipped with stimulus lights and photo beams to record responses. The food tray was connected to a pellet dispenser that delivered 45-mg sucrose pellets (Sandown Scientific, Middlesex, UK). The chambers were controlled by a software written in Med PC (Med Associates, Inc.). The chambers were cleaned with 10% ethanol solution and allowed to dry in between subjects.

2.6.2 | Habituation and training

The rats were habituated to the chambers on two daily 30-min sessions when sugar pellets were placed in all nose poke holes and in the food tray. Following this, the rGT training started, and the rats had to progress through six levels of increasing complexity. The training schedule is similar to that for the five-choice serial reaction time task and was based on the schedule published by Zeeb et al, but with some modifications.[14] A response in the food tray is needed to start a trial. Firstly, all four holes (Holes 1, 2, 3 and 4) were illuminated, and a response in either of them resulted in one pellet reward. The session was finished when the rat had completed 100 trials or after 30 min. When 100 trials under 30 min had been achieved, the subject went on to the next level where only one response hole was illuminated, and a response had to be made in the correct hole before a one pellet

reward was given. In order to proceed, 100 trials had to be completed with ≥80% correct responses and ≤20% omissions. In the first level, the stimulus light was lit until a response was made. In the following levels, the stimulus duration and time to respond was gradually decreased until they reached 2 s, respectively. The last level of the training was a forced choice rGT that had all the same parameters as the free choice rGT (described in the following section), with the exception that only one response hole was lit and only a response in that hole gave rise to either a pellet reward or a punishing time-out. This was done for seven sessions to make sure that all the choice alternatives had been explored. The time to reach the last level of the rGT training differed between individuals (median: 18.5 training days, min: 11, max: 34).

2.6.3 | rGT

The rGT version used in the present study is the same as previously described.[14] A schematic of the test is shown in Figure 1C. In the rGT, all four holes were lit, and the rat could make a free choice. A trial was initiated by a response in the illuminated food tray. The trial began with a 5-s inter-trial interval (ITI) where the subject had to wait before the four response lights were illuminated and a response could be made. Any response made during the ITI was recorded as a premature response, and the house light turned on for 5 s before another trial could be initiated. If no response was made within 10 s after the response holes were activated, the trial was recorded as an omission, and the tray light was re-illuminated, and a new trial could be initiated. The response holes are associated with different number of pellets, length of punishing time-outs and probabilities of reward or punishment. The contingencies with regard to reward probability, number of pellets and duration of punishing time-outs for the different options were P1 $p = 0.9$, 1 and 5 s; P2 $p = 0.8$, 2 and 10 s; P3 $p = 0.5$, 3 and 30 s; P4 $p = 0.4$, 4 and 40 s. Thus, P2, the response hole with two pellets as reward, is most advantageous and will give rise to the highest number of pellets earned during a session. P4 is the riskiest choice and will give the least number of pellets due to the long duration of punishing time-outs. The task was performed 5 consecutive days per week, and the sessions lasted for 30 min. The percentage of each choice was calculated ((#choice of that option/#completed trials) × 100) for P1, P2, P3 and P4. Premature responses and omissions were recorded as total number during each session. Additional responding in the response holes after a choice had been made was defined as perseverative responses. Perseverative responses were divided into perseverative responses during reward (PRdR) and perseverative responses during punishment (PRdP). To make comparisons possible, the PRdR and PRdP were divided by the number of rewarded trials or punished trials, respectively. Total head entries during punishment (head entries), that is, both response holes and the food tray, were also recorded and divided by the number of punished trials.

The individual gambling strategies were based on stable choice patterns during week 5, and groups were formed as follows: the top quartile in P1 formed the safe group, and the top quartile in P2

formed the strategic group. The risky group included the individuals with P4% > Q3 + 1.5 × IQR (interquartile range). One individual that was an outlier (according to Grubbs' outlier test) in P3% was also included in the risky group, as it increased in P3% every week. The remaining individuals formed the group other.

2.7 | R-fMRI

2.7.1 | Animal preparation for MRI

Animals underwent MRI scanning 4–7 weeks after the completion of rGT. Anaesthesia was induced in a box with 5% isoflurane (1:4 oxygen/air mixture; Isoflo® Vet, Orion Pharma Animal Health, Sollentuna, Sweden), and a subcutaneous catheter was inserted when the animals were anaesthetized. The animals were thereafter placed prone in a stereotactic holder with their head cinched, teeth placed in a tooth bar and a nosecone placed around their nose that provided 2% isoflurane in a mixture of oxygen and air (ratio 1:4). A rectal thermometer, a pulse oximeter and breathing sensor (all SA Instruments, Stony Brook, NY, USA) were used to monitor the animal during the MRI measurements. To maintain a steady body temperature of 37°C, a feedback hot air system (SA Instruments, Stony Brook, NY, USA) was used. When the rat reached a steady core temperature of 37°C, a bolus dose of medetomidine (0.05 mg/kg; Domitor® Vet, Orion Pharma Animal Health, Sollentuna, Sweden) was administered by an infusion pump (PHD 2000 infuse/withdraw, Harvard Apparatus, Holliston, MA, USA) via the subcutaneous catheter. Isoflurane flow was lowered to 0.25% 5 min after the bolus. Fifteen minutes after the reduction of isoflurane flow, a steady flow of medetomidine (0.1 mg/kg/h) was administered by an infusion pump (PHD 2000 infuse/withdraw, Harvard Apparatus, Holliston, MA, USA) until the end of the experiment.

2.7.2 | MRI data acquisition procedure

All MRI measurements were conducted using a 9.4T experimental MRI system (VnmrJ software 3.1, Agilent, Yarnton, UK). The MRI scanner was equipped with a gradient system of 12 cm inner diameter and a maximum strength of 600 mT/m. An actively tuned transmit–receive bird-cage coil of 72 mm ID (RAPID Biomedical GmbH, Wüzburg-Rimpar, Germany) was utilized for the volumetric scanning of the brain anatomy. An actively detuned, receiver-only, four-channel phased array surface coil (RAPID Biomedical GmbH, Wüzburg-Rimpar, Germany) was used for rapid data acquisition of R-fMRI based on an echo-planar-imaging (EPI) method. The MRI acquisition protocol included the following:

1. 3D gradient recalled echo (GRE) imaging using the following main acquisition parameters: $50 \times 40 \times 40$ mm^3 field of view (FOV), matrix size $= 128 \times 128 \times 128$ data matrix, TE/TR $= 2.91/1.47$ ms and flip angle $= 20°$.

2. Anatomic reference scans were acquired using a fast spin echo sequence (FSE) with a stack of 11 transverse slices of 1 mm thickness. The positions of the slices were carefully selected so that the anterior commissure joined medially in the central slice. The following settings were used for the scanning: TR $= 3$ s, echo train containing 8 echoes where the fourth echo was localized to the centre of k-space, NEX $= 1$, matrix size $= 256 \times 256$, FOV $= 48 \times 48$ mm^2 and a slice thickness of 1 mm.

3. R-fMRI data were acquired using a single-shot GRE EPI protocol with the following acquisition parameters: FOV $= 32 \times 32$ mm^2, matrix size $= 64 \times 64$, 11 interleaved transverse slices at the same positions as the anatomic reference scan described above, slice thickness $= 1$ mm with no slice gap, TR/TE $= 1000/16.33$ ms, 300 dynamic repetitions with a total acquisition time of 5 min, bandwidth $= 2791$ Hz/pixel and eight dummy scans preceded the data collection in order to achieve signal steady state. For each animal, the R-fMRI data acquisition was repeated twice in the same session.

2.7.3 | R-fMRI data preprocessing

The R-fMRI data underwent the following preprocessing procedures:

1. Rigid-body motion correction. After de-spiking, each R-fMRI time series was aligned to the first volume using a six-parameter model to correct for rigid motion artefacts. Skull stripping based on the average image of each time series was preformed prior to the registration to eliminate ghosting and bone signals outside the brain volume. The skull stripping was preformed manually by using the ITK-SNAP software (www.itksnap.org).[36]

2. Correction of the image distortion associated B$_0$ inhomogeneity. B$_0$ inhomogeneity can affect GRE measurements acquired with single-shot EPI and result in spatially non-linear image distortions. To mitigate such image distortions, we implemented a deformable registration framework based on mutual information metric. The framework can reduce EPI distortions and significantly improve the quality of the blood oxygen level dependent (BOLD) fMRI data. The correction was carried out firstly by co-registering the average image volume for the GRE time series to the corresponding FSE anatomical reference image and then applying the correction parameters to each image volume in the BOLD time series.

3. Spatial normalization of the R-fMRI data sets for individual animals to the intermediate template based on group average. The construction of the group-based intermediate template was performed by selecting a typical rat brain as the initial reference (the average of any BOLD time series), registering the different rat brains (the average of each BOLD time series) to the initial reference and taking average for the registered group data. The spatial normalization to the intermediate template was completed by using a 12-parameter linear affine registration algorithm.

4. Nuisance signal removal. This was performed by voxel-wise regression using 14 regressors based on the motion correction

parameters, average signal of the ventricles and their first-order derivatives.

5. Smoothing and bandpass filtering to suppress signal noise and improve signal-to-noise ratio of the R-fMRI data. After baseline trend removal up to the third-order polynomial, effective bandpass filtering was performed using low-pass filtering at 0.08 Hz. The smoothing of the spatially normalized R-fMRI data was conducted by using a Gaussian kernel with full width at half maximum of 0.65 mm.

The entire preprocessing pipeline was conducted using a shell wrapper based on different C programs of the AFNI (afni.nimh.nih.gov) and FSL (fmrib.ox.ac.uk) software packages.

2.8 | Statistical analyses

2.8.1 | Behavioural data analysis

Statistical analyses were carried out in Statistica 13 (TIBCO Software Inc., Tulsa, OK, USA) unless otherwise specified. Data were considered statistically significant at $p < 0.05$. Parameters were examined for normality using the Shapiro–Wilk W test. The majority of all parameters in the MCSF, novel cage and rGT were not normally distributed; hence, non-parametric statistics were used. Between-subject differences with more than two groups were examined with Kruskal–Wallis analysis of variance (ANOVA) by ranks and post hoc Mann–Whitney U test with continuity correction where appropriate. Between-subject differences with two groups were examined using the Mann–Whitney U test with continuity correction. Analysis of main effects and interactions in non-parametrical, longitudinal data sets from the rGT were carried out in R 3.2.3[37] using the nparLD package[38] with gambling strategy group as between-subject factor and choice as within-subject factor. Between-subject post hoc tests were performed with the Mann–Whitney U test with continuity correction, and within-subject post hoc tests were performed with Wilcoxon's matched pairs test. Outliers in the P3 choice of the rGT were identified with Grubbs' outlier test. The Spearman rank order correlation was used for analysis of correlations.

For the MCSF data, a trend analysis was performed, as previously described.[39] The trend analysis is a rank order procedure that groups descriptive parameters within the same functional behavioural categories. These categories are general activity (total activity, number of visits to the corridors, duration per visit to the corridors [reversed], number of visits to the centre and the total distance moved in the arena), exploratory activity (duration in the corridors [reversed], duration in the centre [reversed], duration in the hurdle, number of rearings and nose-pokes in the hole board holes), risk assessment (SAPs in the centre and number of visits to, duration in and duration per visit in the slope), risk-taking behaviour (number of visits to, duration on and duration per visit on the bridge and number of visits to, duration in and duration per visit to the CTRCI) and shelter-seeking behaviour (number of visits to, duration in and duration per visit to the DCR).

2.8.2 | R-fMRI data analysis

Quantitative data-driven analysis of R-fMRI data

Quantitative data-driven analysis (QDA) reveals changes in general brain connectivity. Every voxel in the brain was used in turn as a seed, and clusters with high connectivity metrics were identified as functional hubs. For QDA, a framework to compute the voxel-wise cross-correlation coefficient matrix of the R-fMRI data was implemented. For each voxel inside the brain, Pearson's cross-correlation coefficients (CC) of the R-fMRI time course with that of every other voxel inside the brain was computed. With the QDA approach, two voxel-wise resting-state functional connectivity (RFC) metrics were derived from the CC matrix, the connectivity strength index (CSI) and connectivity density index (CDI).[40] CSI is defined as the non-zero mean value of the cube of the CC for all voxel pairs involving the current voxel in question, $\text{CSI} = \left(\sum_{CC \neq 0} CC^3 \right) / n$, where n is the total number of voxel pairs with non-zero CC. CSI provides a metric for the local connectivity strength with the rest of the brain, that is, how strong the local voxel is associated with the rest of the brain. CDI is defined as the convolution between the histogram of the CC for all voxel pairs involving the current voxel in question and the kernel function $y = abs(x^3)$ (where $-1.0 \leq x \leq 1.0$), $\text{CDI} = hist(CC) \otimes abs(x^3)$. CDI provides a metric for the local connectivity density with the rest of the brain, that is, how densely the local voxel is associated with the rest of the brain.

Seed-based analysis

The QDA method does not highlight the specific connectivity changes between selected brain regions. To further explore the specific connectivity differences related to the reward networks, a seed-based analysis using the regions of interests (ROIs) detected from the QDA analysis was performed. The seeds were placed at the peaks of the nucleus accumbens clusters detected from the group comparisons of the QDA metrics. The CC map was computed for each animal by using the average time course of the BOLD signals for the selected ROIs as the reference.

2.8.3 | Statistical analysis of R-fMRI data

QDA

To investigate the possible association between the spontaneous brain activities with gambling behaviour, regression analysis of the rGT behaviour data and RFC metrics derived from the R-fMRI measurements was used. For data reduction, a principal component analysis (PCA) was conducted on the rGT behaviour data using the MATLAB software (the MathWorks, Inc., Natick, Massachusetts, USA). The rGT data for all 30 animals (Table S2) were analysed using PCA. The first three PCA components accounted for 95.3% of the variance (the contributions from the respective components were 56.2%, 23.3% and 15.8%, respectively). To further explore the possible links between the intrinsic brain activities and gambling behaviour,

we carried out linear regression analysis of the top two PCA components with the CSI and CDI metrics in a voxel-by-voxel fashion using the AFNI program 3dRegAna. Moreover, voxel-wise two-sample t-test analyses of the CSI and CDI metrics between the different subgroups of animals with different gambling strategies were performed using the AFNI program 3dttest++ to identify RFC metrics unique for the gambling strategy groups. The two-sample t-test procedure was carried out systematically for all possible group combinations among the four subgroups of animals with different gambling strategies. Normalization of regional volumes by intracranial volume (ICV) may influence the assessment of local functional connectivity. Therefore, we conducted voxel-based morphometry analysis with SPM12 software (https://www.fil.ion.ucl.ac.uk/spm/software/spm12/) to derive tissue fractional distributions and ICV. The raw RFC metrics versus ICV adjusted RFC metrics were compared by including ICV as a covariate factor into the regression and t-test analyses.

The statistical significance for the regression analysis and t-test was assessed using a two-step approach. Firstly, a voxel-wise threshold of $p < 0.001$ (uncorrected) to form initial cluster candidates was imposed. Secondly, permutation simulations without assuming a particular form of probability distribution for the voxel values in the RFC metric images were performed to identify the ROIs from the initially detected clusters with significant difference in the RFC metrics at family-wise error rate (FWER) $p \leq 0.05$. That is, a corrected p-value was estimated for each initially identified cluster through the random permutation simulations. Using the detected ROIs as masks, the RFC mean values for the ROIs were evaluated for further analysis in the context of their relevance for the animals' gambling behaviour.

Seed-based analysis

For the derived CC maps associated with the selected nucleus accumbens seed, a one-sample t-test was performed to generate the average connectivity network associated with the selected seeds. Between-group differences were tested with two-sample t-test. The two-sample t-test procedure was carried out systematically for all possible group combinations among the four subgroups of animals with different gambling strategies. The statistical significance of the t-tests was also assessed with FWER $p \leq 0.05$ at cluster level.

2.8.4 | Visualization of the R-fMRI results

An open-access volumetric atlas based on structural MRI of 39-μm isotropic spatial resolution[41] was used as a template to provide detailed anatomical delineations of the rat brain in addition to a rat brain atlas.[42] For the spatial registration of the R-fMRI slab to the whole-brain template, we manually selected an initial location of an axial slab of 11 mm that approximately matched the brain volume for the BOLD R-fMRI measurements from the template. The location of the slab was then systematically incremented through a numerical loop of 100 steps (±50 mm of the initial location) so that the selected final template slab and the intermediate template from the BOLD R-fMRI group average were optimally matched with the minimum difference. The affine registration parameters were then applied to the statistical results from the regression and t-test analyses by using the final template slab as the master reference. The spatially aligned statistical results were resampled to 0.1 mm resolution and overlaid onto the template brain for visualization.

3 | RESULTS

3.1 | rGT and behaviour

The progression of choices in the rGT over the weeks is shown in Figure S2 and Table S3. Individual differences in gambling strategies revealed a stable pattern. From week 3 onwards, P2 was the preferred option for the population as a whole (Table S3). However, individual differences in choice of the different options started to emerge during week 3 and remained stable for the rest of the experiment (Figure S2).

Based on performance during week 5, the groups safe ($n = 6$), strategic ($n = 8$) and risky ($n = 7$) were formed. The remaining individuals constituted the group other ($n = 11$; Figure 2A). The following presentation of the rGT results focus on the risky, safe and strategic rats.

There were main effects ($p < 0.001$) of gambling strategy group (risky, strategic and safe) and choice (% P1, P2, P3 and P4) as well as an interaction ($p < 0.001$) between gambling strategy group and choice. The choices within the respective groups revealed different patterns (Figure 2B–D). The risky group chose P2 more than P3 (Figure 2B). The strategic group chose P2 more than any other option and P1 more than P3 and P4 (Figure 2C). Finally, the safe group chose P1 more than P3 and P4, P2 more than P4 and P3 more than P4 (Figure 2D). When comparing differences in choices between the groups (Figure 2E–H), rats in the risky group chose P1 and P3 fewer times and P4 more times than the safe group (Figure 2E,G,H). Moreover, the risky group chose P2 fewer times and P4 more times than the strategic group (Figure 2F,H). The strategic group choose P1 and P3 fewer times and P2 more times than the safe group (Figure 2E–G).

Further parameters derived from the rGT are shown in Table S4. The risky rats had shorter latency in first collecting the reward than the safe rats, but not relative to the strategic rats. Moreover, the risky group made more perseverative responses during reward than rats in the strategic and safe group, respectively. Finally, the strategic group made more omissions than the risky and safe group, respectively (Table S4). The validation of the gambling strategy groups is shown in Supporting Information, p.7, and Figure S3.

The body weight was closely monitored during the weeks of restricted feeding (Figure 1A) and did not differ between the gambling strategy groups during rGT (Table S4).

No differences in behaviour in the MCSF or novel cage tests between the gambling strategy groups were observed (Supporting Information, p. 8, Figure S4, Tables S5 and S6).
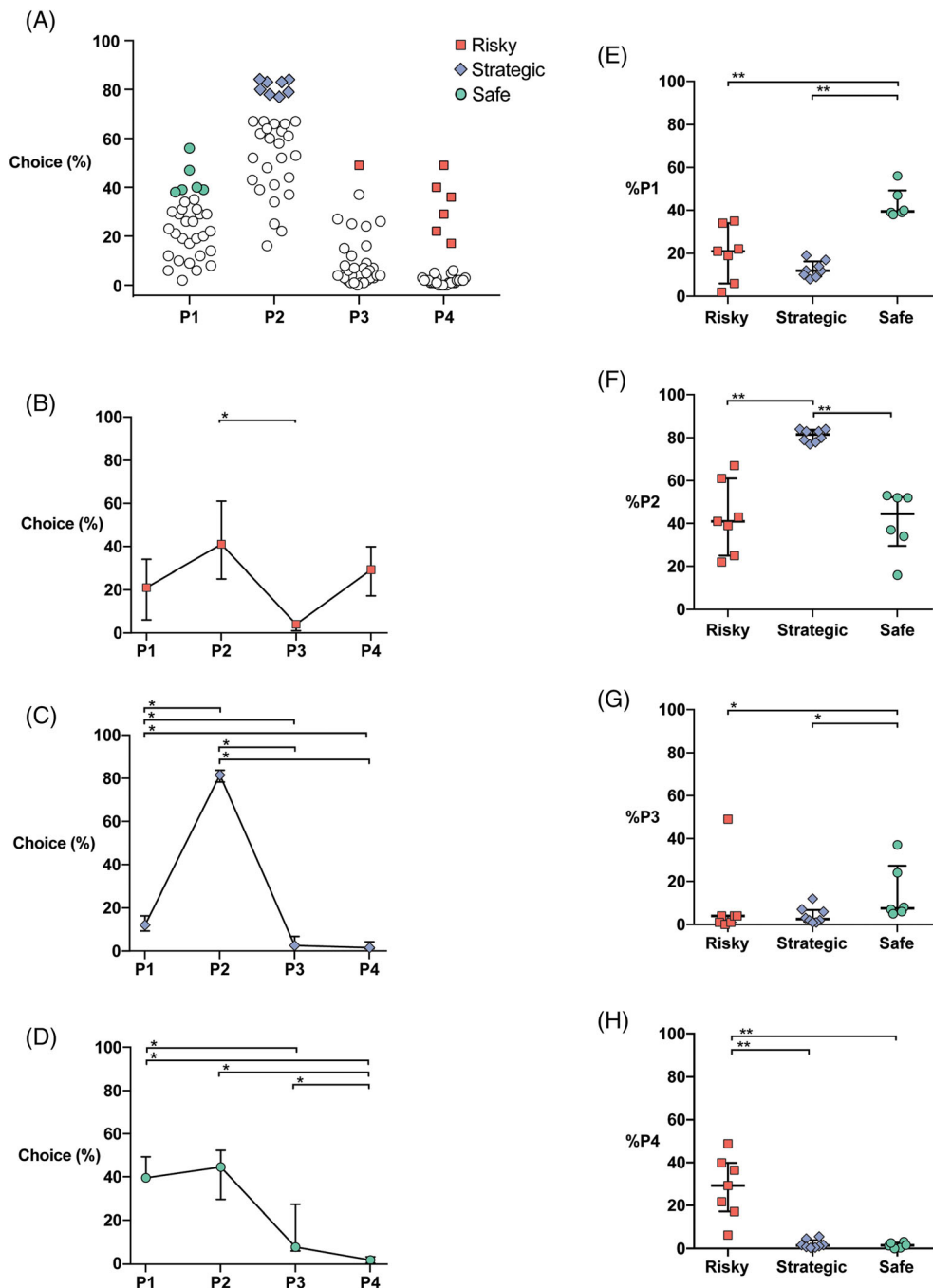
FIGURE 2 Results from the rGT. (A) Distribution of the choices in the population tested ($n = 32$), with choices in per cent on the y-axis and the four available choices (P1–P4) on the x-axis. The individuals are coloured by gambling strategy group into safe (green circles), strategic (blue diamonds) and risky (red squares). The groups are only marked out in the choice that distinguishes that strategy group, the uncoloured circles represent all individuals who are not a part of the group being displayed in that choice category. (B–D) Choices of P1, P2, P3 and P4 within the (B) risky ($n = 7$), (C) strategic ($n = 8$) and (D) safe ($n = 6$) rats. Data are presented as median with upper and lower quartiles. $^*p < 0.05$, $^{**}p < 0.01$, $^{***}p < 0.001$ (post hoc Wilcoxon matched pairs test). (E–H) Difference in choice between the gambling strategy groups. Choice (%) of P1 (E), P2 (F), P3 (G) and P4 (H). Individual rats are shown as symbols with group median marked by a line and upper and lower quartiles indicated by whiskers. $^*p < 0.05$, $^{**}p < 0.01$, $^{***}p < 0.001$ (post hoc Mann–Whitney U test)

3.2 | Gambling strategies and R-fMRI

Two-sample t-tests of the voxel-based morphometric analysis results did not show significant differences (FWER, $p < 0.05$) in grey matter volume between any of the gambling strategy groups. The ICV did not scale proportionally with the connectivity metrics in any specific local region, and ICV correction did not significantly change the R-fMRI results in relation to the different gambling strategies.

3.2.1 | QDA

Based on the explorative focus of the study and the novel aspect of investigating gambling strategies using R-fMRI, the group other was incorporated in the analysis of the R-fMRI results. Figure 3A shows the scatter plot of PCA component $t(1)$ versus component $t(2)$ (variance contribution 79.5%) with all animals coloured according to gambling strategy groups. Four clusters could readily be identified, which were associated with animals of different strategy groups in the rGT.
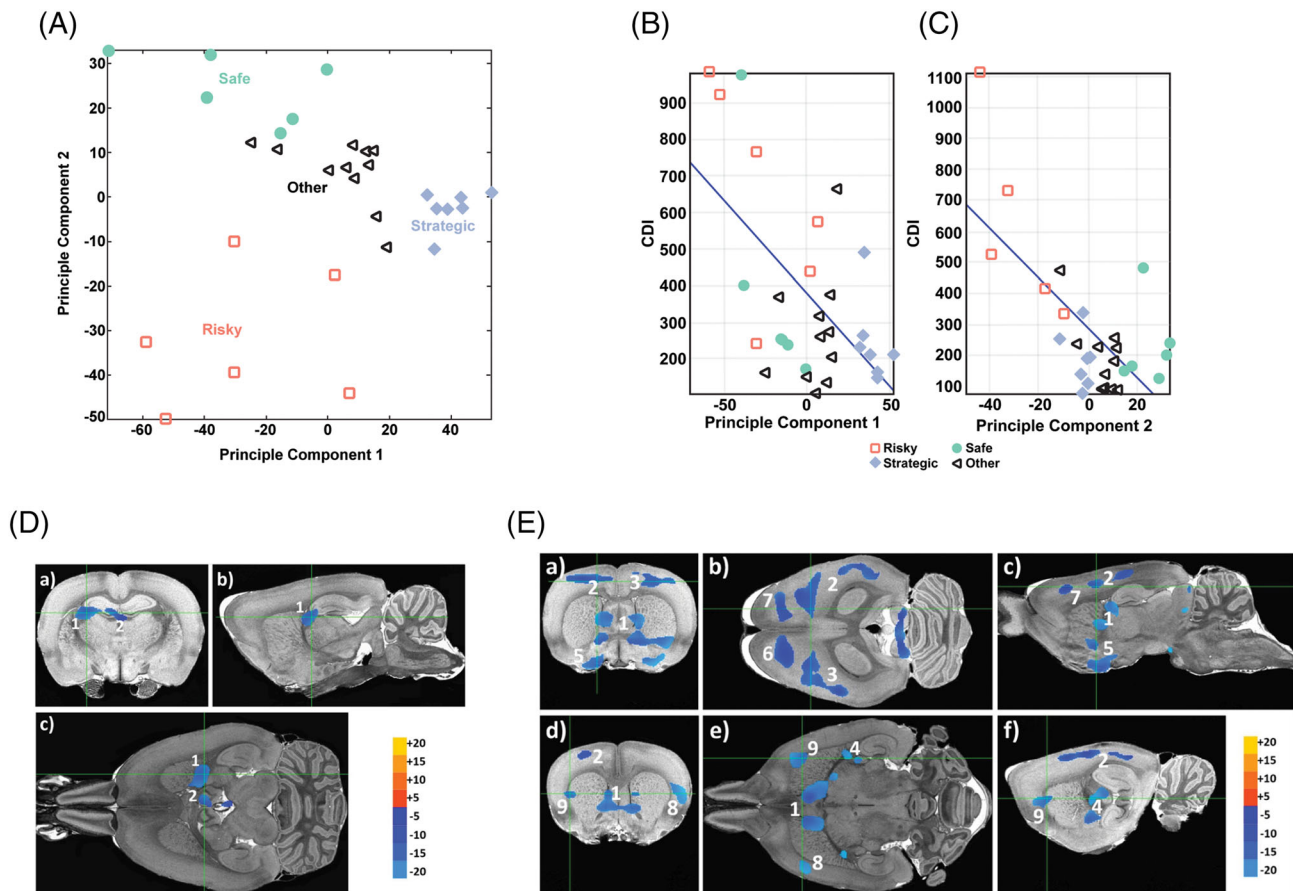
FIGURE 3   (A) Scatter plot of the top two principal components for the 30 animals that underwent the R-fMRI according to gambling strategy group. (B–E) R-fMRI results on a population level. (B) The scatter plot of the average CDI for the ROIs with significant correlation between the CDI metric and principal component $t(1)$. (C) The scatter plot of the average CDI for the ROIs with significant correlation between the CDI metric and principal component $t(2)$. (D) Brain regions with significant correlations ($p \leq 0.05$) between CDI and principal component $t(1)$ shown in three anatomical sections: coronal (A), sagittal (B) and horizontal (C). The green lines indicate the location of the crossing planes. The colour bar shows the scale for the t-score. The numeric annotations indicate the ROIs of different sizes in descending order according to Table 1. (E) Brain regions with significant correlation ($p \leq 0.05$) between CDI and principal component $t(2)$ shown in three anatomical sections: coronal (A and D), sagittal (B and E) and horizontal (C and F). To illustrate all the significant ROIs, cross sections at two different locations are depicted corresponding to the upper and lower rows, respectively. The green lines indicate the locations of the crossing planes. The colour bar shows the scale for the t-score. The numeric annotations indicate the ROIs of different sizes in descending order according to Table 1

The risky group had negative $t(1)$ and $t(2)$ and was located in the lower left quadrant of the graph. Animals in the safe group had low $t(1)$ and the highest $t(2)$ values and formed a cluster in the top of the graph. The strategic group had low $t(2)$ and the highest $t(1)$ values and formed a cluster at the far right of the graph. Finally, the group other loaded in the middle of the graph and had intermediate $t(1)$ and $t(2)$ values. The parameter's contribution to the loading of the individuals are shown in Figure S5. P2 and P2% (strategic) dominated the projection to positive $t(1)$, whereas P1 and P1% dominated the contribution to positive $t(2)$. P4 and P4% (risky) contributed mainly to negative $t(1)$ and $t(2)$.

The CSI metrics showed no significant correlation with the top two PCA components (data not shown), whereas CDI metrics depicted a significant ($p < 0.05$) negative correlation with the top two principal components in a number of brain regions. Figures 3B and 3C shows the regression results for CDI versus principal components

$t(1)$ and $t(2)$, respectively. As summarized in Table 1, the principal component $t(1)$ was negatively correlated with CDI in the hippocampus, caudate putamen, stria terminalis, thalamus and habenula (Figure 3D). Moreover, the principal component $t(2)$ was negatively correlated with CDI in the septum, caudate putamen, nucleus accumbens, primary and secondary motor cortices, primary somatosensory cortices (hindlimb region, forelimb region, upper lip region), thalamus, basal forebrain region, globus pallidus, amygdala, medial forebrain region and ventral pallidum (Figure 3E). The CDI metrics in these brain regions demonstrated a stronger association with the principal component $t(2)$. The correlation coefficients for $t(1)$ and $t(2)$ were -0.62 and -0.73, respectively. The risky gambling group tended to possess low PCA $t(1)$ and high CDI, which was opposite to the strategic group (Figure 3B). The risky group also tended to possess low PCA $t(2)$ and high CDI, which was opposite to the animals in the safe group (Figure 3C).

TABLE 1 Summary of the brain regions of interest (ROIs) with significant correlation ($p \leq 0.05$) between CDI and the top two principal components $t(1)$ and $t(2)$, respectively

PCA	ROI	Size (μl)	p	Anatomic annotation
t (1)	1	2.245	0.05	Hippocampus, caudate putamen, stria terminalis
	2	1.601	0.05	Thalamus, hippocampus, habenula
t (2)	1	43.787	0.01	Septum, caudate putamen, nucleus accumbens
	2	14.968	0.01	Neocortex (M1, M2, S1HL and S1FL)
	3	13.398	0.01	Neocortex (M1, M2, S1HL and S1FL)
	4	5.699	0.03	Thalamus, basal forebrain region, globus pallidus
	5	4.387	0.05	Amygdala, basal forebrain region, medial forebrain region, ventral pallidum
	6	4.157	0.05	Neocortex (M1 and M2)
	7	2.736	0.05	Neocortex (M1 and M2)
	8	1.607	0.05	Neocortex (S1ULp)
	9	1.559	0.05	Caudate putamen, neocortex (S1ULp)

Note: Brain regions were located with the guidance of a rat brain atlas.[42]
Abbreviations: M1, primary motor cortex; M2, secondary motor cortex; S1FL, primary somatosensory cortex, forelimb region; S1HL, primary somatosensory cortex, hindlimb region; S1ULp, primary somatosensory cortex, upper lip region.
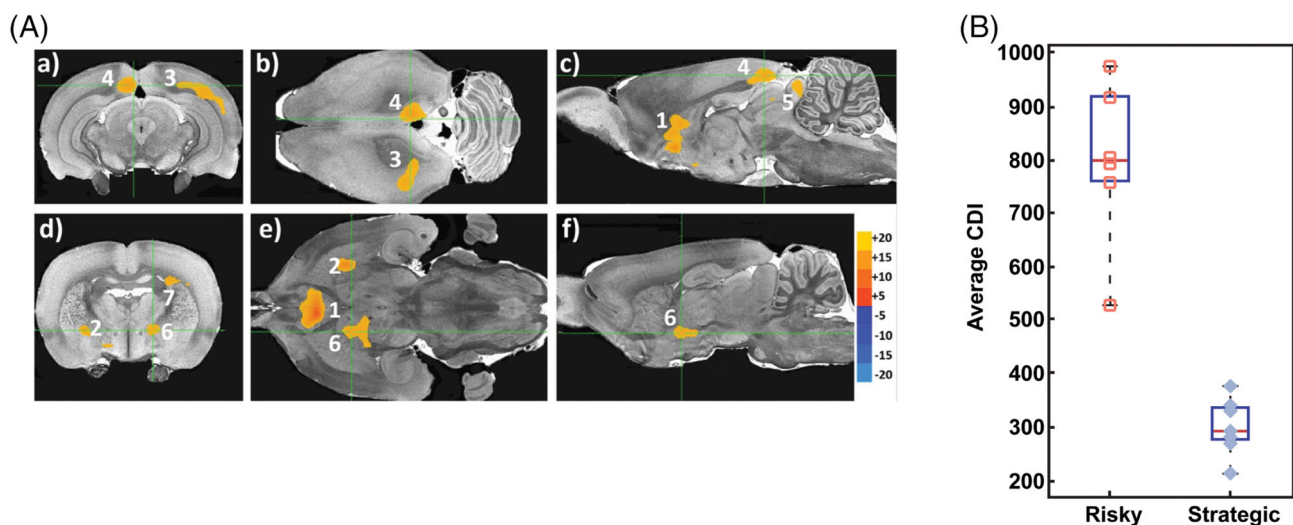

FIGURE 4 R-fMRI results when comparing rats with different gambling strategies. (A) Brain regions with significant difference in CDI ($p \leq 0.05$) between the risky ($n = 6$) and the strategic ($n = 7$) group. The green lines indicate the locations of the crossing sections: coronal (a), sagittal (b) and horizontal (c). The colour bar shows the scale for the t-score. The numeric annotations indicate the ROIs of different sizes in descending order according to Table 2. (B) Box scatter plots of the average CDI metrics for the risky versus strategic rats. The box plots depict the averages for the different subgroups, and the scatters within each box indicate the ROI average for the individual animal in each group

Among all possible pairwise comparisons between the different gambling strategy groups, the risky versus strategic group (Figure 4) and risky versus other group (Supporting Information, p. 15, Figure S6, Table S7) showed significant differences in CDI. There was no significant difference in the CDI metrics between the remaining groups (risky versus safe, strategic versus safe and safe versus other; data not shown). As summarized in Table 2 and shown in Figure 4A, the risky group depicted significantly higher CDI in the caudate putamen, nucleus accumbens, septum, insular cortex, primary somatosensory cortex (upper lip region), bed nucleus of stria terminalis, external part of globus

pallidus, agranular insular cortex and primary motor cortex compared with the strategic rats. The CDI differences between risky and strategic rats are further illustrated by the group averages shown in Figure 4B.

3.2.2 | Seed-based analysis

The results for the seed-based analysis are summarized in Figure 5. The brain functional network associated with the nucleus accumbens is shown in Figure 5A. Besides the prefrontal-striatal circuit, the nucleus

TABLE 2 Summary of the two-sample t-test results for the brain regions of interest (ROIs) with significant differences (FWER, $p \leq 0.05$) in CDI between the risky ($n = 6$) and strategic ($n = 7$) rats

ROI	Size (µl)	p	Anatomic annotation
1	43.787	0.01	Caudate putamen, nucleus accumbens, septum, neocortex (insular cortex)
2	14.968	0.01	Neocortex (S1ULp, insular cortex), caudate putamen
3	13.398	0.01	Caudate putamen, bed nucleus of stria terminalis, EGP
4	5.699	0.05	Caudate putamen, septum
5	4.718	0.05	Neocortex (AI)
6	4.387	0.04	Neocortex (S1ULp)
7	4.157	0.04	Neocortex (M1)

Note: Brain regions were located with the guidance of a rat brain atlas.[42]
Abbreviations: A1, agranular insular cortex; EGP, external part of globus pallidus; M1, primary motor cortex; S1ULp, primary somatosensory cortex, upper lip region.
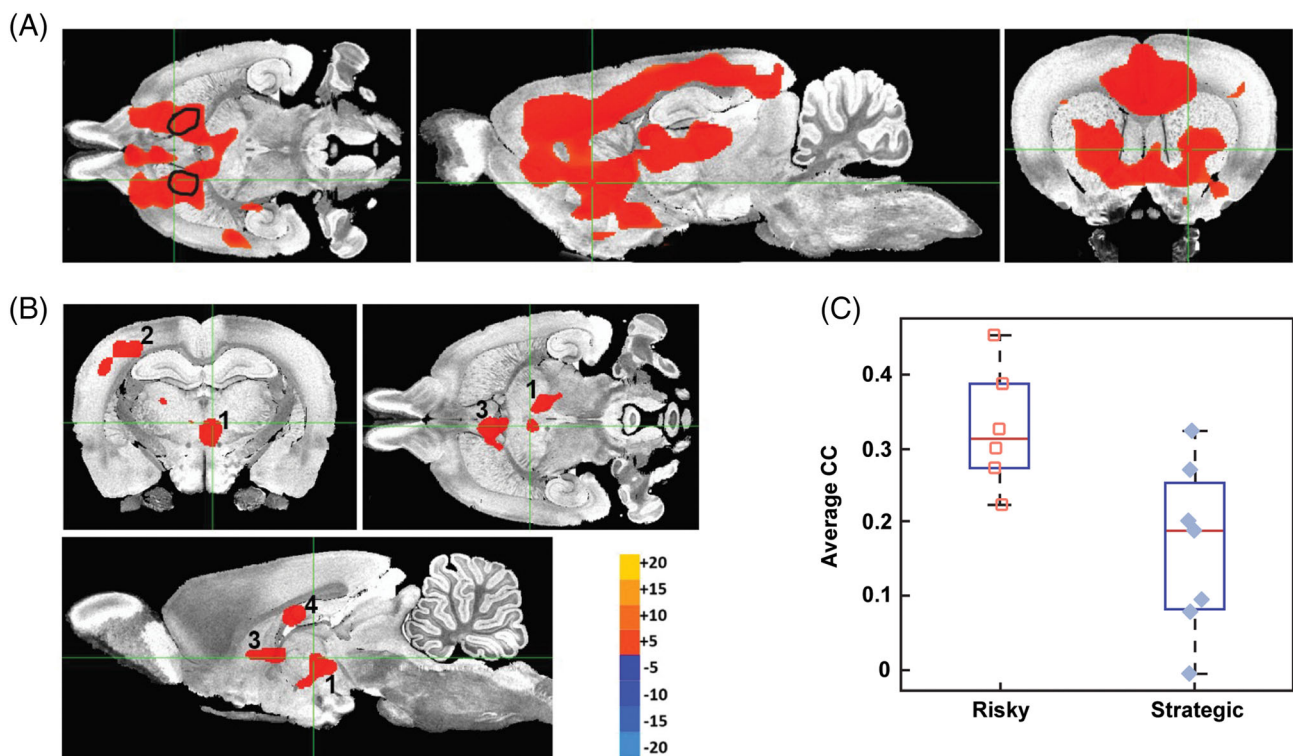

FIGURE 5 Summary of R-fMRI results for the seed-based analysis. The encircled areas indicate the seed locations, the green lines indicate the locations of the crossing sections and the colour bar shows the scale for the t-score. (A) Brain regions where the R-fMRI time courses are significantly (FWER, $p \leq 0.05$) associated with the average time course of the seed in the nucleus accumbens as detected with the QDA approach. (B) Brain regions with significant difference in CC associated with the average time course of the seed (FWER, $p \leq 0.05$) as detected by two-sample *t*-test between the risky ($n = 6$) and strategic ($n = 7$) rats. The numeric annotations indicate the ROIs of different sizes in descending order according to Table 3. (C) Box scatter plots of the average CC of animals in the risky versus strategy groups. The box plots depict the averages for the different subgroups, and the scatters within each box indicate the ROI average for the individual animal in each group

accumbens was also associated with the motor neocortex, thalamus and hippocampus. As shown in Figures 5B and 5C, there were several brain regions with significant differences in the specific functional connectivity associated with nucleus accumbens between the risky and strategic animals. As detailed in Table 3, the involved areas included thalamus, septum, caudate putamen, nucleus accumbens, motor neocortex and hippocampus. Thus, the results for the seed-based analysis depicted similarities with the QDA results (see Figure 3 and Table 2). However, the QDA appeared more sensitive and the t-test results were more extensive (91 vs. 20 µl). There was no significant difference between the remaining groups (risky versus safe, strategic versus safe, strategic versus other and safe versus other; data not shown).

TABLE 3 Summary of the two-sample *t*-test results for the specific connectivity associated with the selected nucleus accumbens seeds. The ROIs are listed in descending order and have significant difference (FWER, $p \leq 0.05$) between the risky ($n = 6$) and strategic ($n = 7$) rats

ROI	Size (μl)	p	Anatomic annotation
1	6.707	0.03	Thalamus
2	6.112	0.03	Neocortex (M1)
3	4.699	0.04	Caudate putamen, septum, nucleus accumbens
4	2.256	0.05	Hippocampus

Note: Brain regions were located with the guidance of a rat brain atlas.[42]
Abbreviation: M1, primary motor cortex.

4 | DISCUSSION

To the best of our knowledge, this is the first study exploring individual differences in gambling strategies in the rGT and associations to behavioural profiles and brain connectivity as assessed by R-fMRI. Stable individual differences in gambling strategies were identified, with subgroups of rats that preferred the suboptimal, safest gambling strategy as well as the disadvantageous, riskiest gambling strategy, and these strategies were associated with distinct variations in functional connectivity in brain regions central for brain reward networks.

4.1 | Gambling strategies in the rGT

In the literature, studies on individual differences in gambling strategies over time are scarce. Herein, it was revealed that individual differences in choice patterns became visible during the third week of rGT and remained stable throughout the study. The most advantageous choice (P2) was the preferred choice on a group level, which agrees with previous studies using the same rGT version.[14,43]

Individuals with the most extreme gambling phenotypes were identified and formed the safe, strategic and risky groups. The outcome for the risky individuals proved to be the worst as they had a lower number of rewarded trials and longer time-outs per trial and earned the least cumulative number of pellets. In contrast, the strategic group had the highest number of pellets per trial and a higher number of cumulative pellets earned than the risky group. In studies using the rGT, groups are commonly formed using the sum of the advantageous and the disadvantageous choices, respectively.[14,43] However, because this approach adds together different choices, it cannot be used to identify the individuals that are most extreme in their choices, with potentially different underlying neurobiology also between extremes in P1 and P2, as indicated by the PCA and subsequent regression analysis herein.

4.2 | Brain functional connectivity in rats with different gambling strategies

Decision-making depends on a complex interplay between several neural systems. The PCA based upon the rGT parameters revealed a clear separation between the gambling strategy groups with significant correlations in brain connectivity in brain regions including the hippocampus, nucleus accumbens, caudate putamen, stria terminalis, septum, habenula, amygdala and thalamus. These brain regions are central for brain reward networks and implicated in motivation, reward and reinforcement and decision-making, as well as different stages of the addiction process.[44,45] Moreover, the findings herein are in agreement with a human study on healthy volunteers performing the IGT during fMRI scanning that revealed activity in areas including the dorsolateral prefrontal cortex, cingulate cortex and nucleus accumbens, but not the hippocampus and amygdala.[30] The importance of the amygdala has however been shown in other studies on decision-making processes as measured by the IGT.[46,47]

Based on the QDA and seed-based analyses, the risky rats differed from the strategic and, based on QDA only, also the group other. The risky gambling strategy was correlated with higher CDI in the nucleus accumbens, caudate putamen and amygdala and higher CC in caudate putamen and nucleus accumbens. This agrees with findings from studies of patients with GD that reported higher functional connectivity between nucleus accumbens and amygdala[48] as well as increased R-fMRI connectivity in the network including cingulate cortex, caudate nucleus and nucleus accumbens compared with healthy controls.[49] Moreover, a study using a cued version of the rGT showed that inhibition of dopaminergic projections to the nucleus accumbens induced a switch from risky to optimal gambling strategies in male rats.[50] Finally, in a recent study based on a rodent 'blackjack' task and manipulation of the connections between the basolateral amygdala and nucleus accumbens, van Holstein et al investigated how the interactions between the basolateral amygdala and nucleus accumbens promoted non-advantageous choices.[51] The emerging evidence thus support the notion that the amygdala–nucleus accumbens circuitry play an essential role in decision-making.

Results from both QDA and seed-based analysis indicated that the strategic gambling strategies were correlated with lower functional connectivity in the hippocampus, caudate putamen, thalamus and habenula. The low functional connectivity in the hippocampus of the strategic rats was unexpected as it contradicts the demonstrated role of the hippocampus in flexible decision-making.[52] In contrast, our findings resonates with a recent BOLD fMRI study in which activity in the thalamus and caudate was negatively correlated with gambling severity.[20] Moreover, the negative correlation in the habenula is notable based on its critical role in reward-associated learning by modulating dopamine levels[53] and

results demonstrating that deep brain stimulation of the habenula could reduce cocaine and sucrose intake in rats.[54,55]

In healthy volunteers performing different versions of the IGT during fMRI scanning, activity in areas of the prefrontal cortex was revealed.[30] As reviewed by Clark et al, dysregulation in the prefrontal cortex has been identified in numerous fMRI studies on GD, but the direction of the reported differences was inconsistent.[31] The results of the presented study revealed differences in functional connectivity between risky and strategic rats in several cortical areas, including cingulate cortex, but not the medial prefrontal cortical areas with demonstrated involvement in decision-making processes.[56] However, the seed-based analysis detected intrinsic activity associations between nucleus accumbens and prefrontal cortex, but no differences between the strategy groups. This is likely due to the limited number of animals in each gambling subgroup. It may also explain the lack of CSI related findings, as differences in CSI have been reported in previous rodent[57] and human[58] studies with sufficient statistical power.

4.2.1 | Methodological considerations

There is currently no consensus as to which normalization approach is optimal. The residual correction by including ICV as a covariate effectively eliminated the correlation between the RFC and ICV. However, as expected, the association between RFC and gambling strategies was not altered by the ICV normalization.

In this study, we applied the QDA framework. The QDA metrics can identify connectivity hubs and assess the general connectivity with the rest of the brain without specifying a specific path or network. The seed-based analysis has been widely used for R-fMRI, and the connectivity between specific regions is explicitly tested in a model-driven framework. Unlike atlas-based ROI definitions, we used an ROI defined from the QDA results. This can potentially improve the accuracy and sensitivity of the seed-based analysis and, as shown herein, further strengthened some of the results from the QDA.

4.3 | Gambling strategies are not related to behavioural profiles

To our knowledge, this is the first time that this version of the rGT has been combined with exploration-based behavioural tests. Surprisingly, no associations between behavioural profiles and explorative strategies, assessed using the MCSF and novel cage tests, respectively, and gambling strategies were found. This contrasts previous work where the MCSF was useful in revealing associations between risk-related behaviour and voluntary alcohol intake.[28,59] Human data reveal that patients with GD expressed a more risk-taking behaviour,[19,20] though diverging results regarding risk-taking behaviour have been found in rodents. Some studies have revealed that risk-taking differs between good decision makers and poor decision makers,[22–24] whereas others have not found this relationship.[21] Such

discrepancies in results could be due to the use of different rGT versions or methods used to measure risk-taking behaviour.

4.4 | General discussion

Traits of impulsivity and gambling proneness have been found to be correlated in rats[12,60,61] as well as in humans.[12,62,63] In previous studies using the rGT, no associations between motor impulsivity and decision-making were revealed.[14,64,65] However, a recent meta-analysis demonstrated a negative correlation between advantageous choices and premature responses.[43] This agrees with the finding herein that the strategic rats had lower premature responses than the safe and risky groups, albeit not statistically significant.

Data on the distribution into advantageous or disadvantageous gambling strategies in the general population are scarce. In previous studies using the IGT, nearly half of the subjects failed to learn the advantageous decks,[30] and impaired performance has been shown to range from 11% to 65% depending on scoring method.[66–68] The percentage of rats with risky gambling strategies in the present study, where all rats performed the rGT, was 22%, which corresponds well to the human literature.

It cannot be completely ruled out that the R-fMRI pattern characterizing the risky rats is caused by performing the rGT. However, the detected areas herein cohere with regions found to be significant for human volunteers engaging in the IGT[30] as well as for GD patients.[20,48,49] Additionally, the brain functional connectivity networks are largely stable and suggested to be innate.[32] Based on these considerations, it is tempting to speculate that certain individual differences are predisposing a risky gambling strategy that may lead to problem gambling and GD.

4.5 | Conclusion

In this explorative study, stable individual differences in gambling strategies were found with subgroups of rats that preferred the suboptimal safest choice as well as the disadvantageous choice. Moreover, R-fMRI results provided evidence that individual differences in gambling strategies were associated with regions in or associated with brain reward networks.

CONFLICT OF INTEREST

The authors declare that this study was performed in the absence of conflicts of interest.

AUTHOR CONTRIBUTIONS

Nikita Tjernström: Investigation, data curation, formal analysis, visualization, writing—original draft, review and editing. **Tie-Qiang Li**: Data curation, formal analysis, visualization, writing—review and editing. **Sarah Holst**: Supervision, conceptualization, writing—review and editing. **Erika Roman**: Funding acquisition, supervision, conceptualization, methodology, writing—review and editing.

DATA AVAILABILITY STATEMENT

The data that support the findings of this study are available from the corresponding author upon request.

ORCID

Nikita Tjernström https://orcid.org/0000-0002-4013-5220
Erika Roman https://orcid.org/0000-0001-5418-8289

REFERENCES

1. Calado F, Griffiths MD. Problem gambling worldwide: an update and systematic review of empirical research (2000–2015). *J Behav Addict*. 2016;5(4):592-613.

2. American Psychiatric Association. *Diagnostic and Statistical Manual of Mental Disorders (DSM-5®)*. 5th ed. American Psychiatric Pub; 2013.

3. Grant JE, Odlaug BL, Chamberlain SR. Neural and psychological underpinnings of gambling disorder: a review. *Prog Neuropsychopharmacol Biol Psychiatry*. 2016;65:188-193.

4. Grant JE, Chamberlain SR. Gambling disorder and its relationship with substance use disorders: implications for nosological revisions and treatment. *Am J Addict*. 2015;24(2):126-131.

5. Kraus SW, Etuk R, Potenza MN. Current pharmacotherapy for gambling disorder: a systematic review. *Expert Opin Pharmacother*. 2020; 21(3):287-296.

6. Wareham JD, Potenza MN. Pathological gambling and substance use disorders. *Am J Drug Alcohol Abuse*. 2010;36(5):242-247.

7. Fauth-Bühler M, Mann K, Potenza MN. Pathological gambling: a review of the neurobiological evidence relevant for its classification as an addictive disorder. *Addict Biol*. 2017;22(4):885-897.

8. Bechara A, Damasio AR, Damasio H, Anderson SW. Insensitivity to future consequences following damage to human prefrontal cortex. *Cognition*. 1994;50(1):7-15.

9. Ciccarelli M, Griffiths MD, Nigro G, Cosenza M. Decision making, cognitive distortions and emotional distress: a comparison between pathological gamblers and healthy controls. *J Behav Ther Exp Psychiatry*. 2017;54:204-210.

10. Brevers D, Bechara A, Cleeremans A, Noel X. Iowa gambling task (IGT): twenty years after – gambling disorder and IGT. *Front Psychol*. 2013;4:1-14.

11. Goudriaan AE, Oosterlaan J, de Beurs E, van den Brink W. Decision making in pathological gambling: a comparison between pathological gamblers, alcohol dependents, persons with Tourette syndrome, and normal controls. *Cogn Brain Res*. 2005;23(1):137-151.

12. van den Bos R, Davies W, Dellu-Hagedorn F, et al. Cross-species approaches to pathological gambling: a review targeting sex differences, adolescent vulnerability and ecological validity of research tools. *Neurosci Biobehav Rev*. 2013;37(10):2454-2471.

13. de Visser L, Homberg JR, Mitsogiannis M, et al. Rodent versions of the Iowa gambling task: opportunities and challenges for the understanding of decision-making. *Front Neurosci*. 2011;5:1-21.

14. Zeeb FD, Robbins TW, Winstanley CA. Serotonergic and dopaminergic modulation of gambling behavior as assessed using a novel rat gambling task. *Neuropsychopharmacology*. 2009;34(10):2329-2343.

15. Zeeb FD, Winstanley CA. Lesions of the basolateral amygdala and orbitofrontal cortex differentially affect acquisition and performance of a rodent gambling task. *J Neurosci*. 2011;31(6):2197-2204.

16. Adams WK, Vonder Haar C, Tremblay M, et al. Deep-brain stimulation of the subthalamic nucleus selectively decreases risky choice in risk-preferring rats. *eNeuro*. 2017;4(4):1-13.

17. Adams WK, Barkus C, Ferland J-MN, Sharp T, Winstanley CA. Pharmacological evidence that 5-HT2C receptor blockade selectively improves decision making when rewards are paired with audiovisual cues in a rat gambling task. *Psychopharmacology (Berl)*. 2017;234(20):3091-3104.

18. Rivalan M, Coutureau E, Fitoussi A, Dellu-Hagedorn F. Inter-individual decision-making differences in the effects of cingulate, orbitofrontal, and prelimbic cortex lesions in a rat gambling task. *Front Behav Neurosci*. 2011;5:1-10.

19. Brand M, Kalbe E, Labudda K, Fujiwara E, Kessler J, Markowitsch HJ. Decision-making impairments in patients with pathological gambling. *Psychiatry Res*. 2005;133(1):91-99.

20. Limbrick-Oldfield EH, Mick I, Cocks RE, et al. Neural and neurocognitive markers of vulnerability to gambling disorder: a study of unaffected siblings. *Neuropsychopharmacology*. 2020;45(2):292-300.

21. Alonso L, Peeva P, Ramos-Prats A, Alenina N, Winter Y, Rivalan M. Inter-individual and inter-strain differences in cognitive and social abilities of Dark Agouti and Wistar Han rats. *Behav Brain Res*. 2020; 377:112188.

22. Koot S, Zoratto F, Cassano T, et al. Compromised decision-making and increased gambling proneness following dietary serotonin depletion in rats. *Neuropharmacology*. 2012;62(4):1640-1650.

23. Rivalan M, Ahmed SH, Dellu-Hagedorn F. Risk-prone individuals prefer the wrong options on a rat version of the Iowa gambling task. *Biol Psychiatry*. 2009;66(8):743-749.

24. Rivalan M, Valton V, Seriès P, Marchand AR, Dellu-Hagedorn F. Elucidating poor decision-making in a rat gambling task. *PLoS ONE*. 2013; 8(12):e82052.

25. Meyerson BJ, Augustsson H, Berg M, Roman E. The concentric square field: a multivariate test arena for analysis of explorative strategies. *Behav Brain Res*. 2006;168(1):100-113.

26. Roman E, Colombo G. Lower risk taking and exploratory behavior in alcohol-preferring sP rats than in alcohol non-preferring sNP rats in the multivariate concentric square field™ (MCSF) test. *Behav Brain Res*. 2009;205(1):249-258.

27. Magara S, Holst S, Lundberg S, Roman E, Lindskog M. Altered explorative strategies and reactive coping style in the FSL rat model of depression. *Front Behav Neurosci*. 2015;9:89.

28. Momeni S, Sharif M, Ågren G, Roman E. Individual differences in risk-related behaviors and voluntary alcohol intake in outbred Wistar rats. *Behav Pharmacol*. 2014;25(3):206-215.

29. Palm S, Momeni S, Lundberg S, Nylander I, Roman E. Risk-assessment and risk-taking behavior predict potassium- and amphetamine-induced dopamine response in the dorsal striatum of rats. *Front Behav Neurosci*. 2014;8:236.

30. Li X, Lu Z, D'Argembeau A, Ng M, Bechara A. The Iowa gambling task in fMRI images. *Hum Brain Mapp*. 2009;31(3):410-423.

31. Clark L, Boileau I, Zack M. Neuroimaging of reward mechanisms in gambling disorder: an integrative review. *Mol Psychiatry*. 2019;24(5):674-693.

32. Gratton C, Laumann TO, Nielsen AN, et al. Functional brain networks are dominated by stable group and individual factors, not cognitive or daily variation. *Neuron*. 2018;98(2):439-452.

33. Sierakowiak A, Monnot C, Aski SN, et al. Default mode network, motor network, dorsal and ventral basal ganglia networks in the rat brain: comparison to human networks using resting state-fMRI. *PLoS ONE*. 2015;10(3):e0120345.

34. Hutchison RM, Mirsattari SM, Jones CK, Gati JS, Leung LS. Functional networks in the anesthetized rat brain revealed by independent component analysis of resting-state FMRI. *J Neurophysiol*. 2010;103(6):3398-3406.

35. Arts JW. Effects of reversing light-dark cycle following transfer and re-housing on behavioural and physiological parameters in rats. In Transportation in Laboratory Rats: Effects of a Black Box. Dissertation. Utrecht University: Utrecht University Repository. https://dspace.library.uu.nl/handle/1874/331183. Published online 2016.

36. Yushkevich PA, Piven J, Hazlett HC, et al. User-guided 3D active contour segmentation of anatomical structures: Significantly improved efficiency and reliability. *Neuroimage*. 2006;31(3):1116-1128.

37. R Core Team. R: a language and environment for statistical computing. R Foundation for Statistical Computing; 2018. http://www.R-project.org/

38. Noguchi K, Gel YR, Brunner E, Konietschke F. nparLD: an R software package for the nonparametric analysis of longitudinal data in factorial experiments. *J Stat Softw*. 2012;50(12):1-23.

39. Meyerson BJ, Jurek B, Roman E. A rank-order procedure applied to an ethoexperimental behavior model—the multivariate concentric square field™ (MCSF) test. *J Behav Brain Sci*. 2013;3(4):350-361.

40. Li X, Fischer H, Manzouri A, Månsson KNT, Li T-Q. Dataset of whole-brain resting-state fMRI of 227 young and elderly adults acquired at 3T. *Data Brief*. 2021;38:107333.

41. Kjonigsen LJ, Lillehaug S, Bjaalie JG, Witter MP, Leergaard TB. Waxholm space atlas of the rat brain hippocampal region: three-dimensional delineations based on magnetic resonance and diffusion tensor imaging. *Neuroimage*. 2015;108:441-449.

42. Paxinos G, Watson C. *Paxinos and Watson's The Rat Brain in Stereotaxic Coordinates*. 7th ed. Elsevier Academic Press; 2014.

43. Barrus MM, Hosking JG, Zeeb FD, Tremblay M, Winstanley CA. Disadvantageous decision-making on a rodent gambling task is associated with increased motor impulsivity in a population of male rats. *J Psychiatry Neurosci JPN*. 2015;40(2):108-117.

44. Everitt BJ, Robbins TW. Drug addiction: updating actions to habits to compulsions ten years on. *Annu Rev Psychol*. 2016;67(1):23-50.

45. Koob GF, Volkow ND. Neurobiology of addiction: a neurocircuitry analysis. *Lancet Psychiatry*. 2016;3(8):760-773.

46. Bechara A. Disturbances of emotion regulation after focal brain lesions. *Int Rev Neurobiol*. 2004;62:159-193.

47. Bechara A, Damasio AR. The somatic marker hypothesis: a neural theory of economic decision. *Games Econ Behav*. 2005;52(2):336-372.

48. Genauck A, Matthis C, Andrejevic M, et al. Neural correlates of cue-induced changes in decision-making distinguish subjects with gambling disorder from healthy controls. *Addict Biol*. 2020;26(3):e12951.

49. Piccoli T, Maniaci G, Collura G, et al. Increased functional connectivity in gambling disorder correlates with behavioural and emotional dysregulation: evidence of a role for the cerebellum. *Behav Brain Res*. 2020;390:112668.

50. Hynes TJ, Ferland J-MM, Feng TL, et al. Chemogenetic inhibition of dopaminergic projections to the nucleus accumbens has sexually dimorphic effects in the rat gambling task. *Behav Neurosci*. 2020;134(4):309-322.

51. van Holstein M, MacLeod PE, Floresco SB. Basolateral amygdala – nucleus accumbens circuitry regulates optimal cue-guided risk/reward decision making. *Prog Neuropsychopharmacol Biol Psychiatry*. 2020;98:109830.

52. Rubin RD, Watson PD, Duff MC, Cohen NJ. The role of the hippocampus in flexible cognition and social behavior. *Front Hum Neurosci*. 2014;8:742.

53. Velasquez KM, Molfese DL, Salas R. The role of the habenula in drug addiction. *Front Hum Neurosci*. 2014;8:1-10.

54. Friedman A, Lax E, Dikshtein Y, et al. Electrical stimulation of the lateral habenula produces an inhibitory effect on sucrose self-administration. *Neuropharmacology*. 2011;60(2):381-387.

55. Friedman A, Lax E, Dikshtein Y, et al. Electrical stimulation of the lateral habenula produces enduring inhibitory effect on cocaine seeking behavior. *Neuropharmacology*. 2010;59(6):452-459.

56. Pattij T, Vanderschuren LJMJ. The neuropharmacology of impulsive behaviour. *Trends Pharmacol Sci*. 2008;29(4):192-199.

57. Sierakowiak A. Experimental magnetic resonance imaging modalities as tools to evaluate brain function, structure and networks: exercise and cocaine induced adaptations. Published online 2015.

58. Nordin LE, Möller MC, Julin P, Bartfai A, Hashim F, Li T-Q. Post mTBI fatigue is associated with abnormal brain functional connectivity. *Sci Rep*. 2016;6:1-12.

59. Momeni S, Roman E. Subgroup-dependent effects of voluntary alcohol intake on behavioral profiles in outbred Wistar rats. *Behav Brain Res*. 2014;275:288-296.

60. Adriani W, Boyer F, Gioiosa L, Macrì S, Dreyer J-L, Laviola G. Increased impulsive behavior and risk proneness following lentivirus-mediated dopamine transporter over-expression in rats' nucleus accumbens. *Neuroscience*. 2009;159(1):47-58.

61. Cho BR, Kwak MJ, Kim WY, Kim J-H. Impulsive action and impulsive choice are differentially expressed in rats depending on the age at exposure to a gambling task. *Front Psych*. 2018;9:503.

62. Grant JE, Chamberlain SR. Impulsive action and impulsive choice across substance and behavioral addictions: Cause or consequence? *Addict Behav*. 2014;39(11):1632-1639.

63. Ioannidis K, Hook R, Wickham K, Grant JE, Chamberlain SR. Impulsivity in gambling disorder and problem gambling: a meta-analysis. *Neuropsychopharmacology*. 2019;44(8):1354-1361.

64. Baarendse PJJ, Winstanley CA, Vanderschuren LJMJ. Simultaneous blockade of dopamine and noradrenaline reuptake promotes disadvantageous decision making in a rat gambling task. *Psychopharmacology (Berl)*. 2013;225(3):719-731.

65. Zeeb FD, Wong AC, Winstanley CA. Differential effects of environmental enrichment, social-housing, and isolation-rearing on a rat gambling task: dissociations between impulsive action and risky decision-making. *Psychopharmacology (Berl)*. 2013;225(2):381-395.

66. Barnhart WR, Buelow MT. The performance of college students on the Iowa gambling task: differences between scoring approaches. *Assessment*. 2021;10731911211004740.

67. Bechara A. *Iowa Gambling Task Professional Manual*. Psychological Assessment Resources; 2007.

68. Steingroever H, Wetzels R, Horstmann A, Neumann J, Wagenmakers E-J. Performance of healthy participants on the Iowa gambling task. *Psychol Assess*. 2013;25(1):180-193.

SUPPORTING INFORMATION

Additional supporting information may be found in the online version of the article at the publisher's website.